Letter

Search for the decay $B^0 o \gamma \gamma$ using Belle and Belle II data

I. Adachi, L. Aggarwal, H. Aihara, N. Akopov, A. Aloisio, S. Al Said, N. Althubiti, N. Anh Ky, D. M. Asner, H. Atmacan, T. Aushev, V. Aushev, M. Aversano, R. Ayad, V. Babu, H. Bae, S. Bahinipati, P. Bambade[®], Sw. Banerjee[®], S. Bansal[®], M. Barrett[®], J. Baudot[®], A. Baur[®], A. Beaubien[®], F. Becherer[®], J. Becker[®], K. Belous[®], J. V. Bennett[®], F. U. Bernlochner[®], V. Bertacchi[®], E. Bertholet[®], M. Bessner[®], S. Bettarini[®], B. Bhuyan[®], F. Bianchi, L. Bierwirth, T. Bilka, D. Biswas, A. Bobrov, D. Bodrov, A. Bolz, J. Borah, A. Boschetti, A. Bozek, M. Bračko, P. Branchini, R. A. Briere, T. E. Browder, A. Budano, S. Bussino, Q. Campagna, M. Campajola[®], L. Cao[®], G. Casarosa[®], C. Cecchi[®], J. Cerasoli[®], M.-C. Chang[®], P. Chang[®], P. Cheema[®], C. Chen[®], B. G. Cheon, K. Chilikin, K. Chirapatpimol, H.-E. Cho, K. Cho, S.-J. Cho, S.-K. Choi, S. Choudhury, L. Corona[®], J. X. Cui[®], F. Dattola[®], E. De La Cruz-Burelo[®], S. A. De La Motte[®], G. De Nardo[®], M. De Nuccio[®], G. De Pietro, R. de Sangro, M. Destefanis, S. Dey, R. Dhamija, A. Di Canto, F. Di Capua, J. Dingfelder, Z. Doležal[®], I. Domínguez Jiménez[®], T. V. Dong[®], M. Dorigo[®], D. Dorner[®], K. Dort[®], D. Dossett[®], S. Dreyer[®], S. Dubey, K. Dugic, G. Dujany, P. Ecker, M. Eliachevitch, D. Epifanov, P. Feichtinger, T. Ferber, T. Fillinger[®], C. Finck[®], G. Finocchiaro[®], A. Fodor[®], F. Forti[®], A. Frey[®], B. G. Fulsom[®], E. Ganiev[®], M. Garcia-Hernandez, G. Gaudino, V. Gaur, A. Gaz, A. Gellrich, G. Ghevondyan, D. Ghosh, H. Ghumaryan[®], G. Giakoustidis[®], R. Giordano[®], A. Giri[®], A. Glazov[®], B. Gobbo[®], R. Godang[®], O. Gogota[®], P. Goldenzweig , W. Gradlo, E. Grazianio, D. Greenwaldo, Z. Gruberoyáo, T. Guo, K. Gudkoyao, I. Haideo, Y. Hano, T. Hara, C. Harris, K. Hayasaka, H. Hayashii, S. Hazra, C. Hearty, M. T. Hedges, A. Heidelbach, I. Heredia de la Cruz[®], M. Hernández Villanueva[®], T. Higuchi[®], M. Hoek[®], M. Hohmann[®], P. Horak[®], C.-L. Hsu[®], T. Humair[®], T. Iijima[®], K. Inami[®], N. Ipsita[®], A. Ishikawa[®], R. Itoh[®], M. Iwasaki[®], P. Jackson[®], W. W. Jacobs[®], D. E. Jaffe, E.-J. Jang, S. Jia, Y. Jin, A. Johnson, K. K. Joo, H. Junkerkalefeld, D. Kalita, A. B. Kaliyar, J. Kandra, K. H. Kang, S. Kang, G. Karyan, T. Kawasaki, F. Keil, C. Kiesling, C.-H. Kim, D. Y. Kim, K.-H. Kim[®], Y.-K. Kim[®], H. Kindo[®], K. Kinoshita[®], P. Kodyš[®], T. Koga[®], S. Kohani[®], K. Kojima[®], A. Korobov[®], S. Korpar[®], E. Kovalenko[®], R. Kowalewski[®], P. Križan[®], P. Krokovny[®], T. Kuhr[®], Y. Kulii[®], J. Kumar[®], R. Kumar[®], K. Kumara[®], T. Kunigo[®], A. Kuzmin[®], Y.-J. Kwon[®], S. Lacaprara[®], K. Lalwani[®], T. Lam[®], J. S. Lange[®], M. Laurenza, R. Leboucher, M. J. Lee, C. Lemettais, P. Leo, D. Levit, L. K. Li, S. X. Li, Y. Li, Y. B. Li, Y. B. Li, J. Libby[®], Z. Liptak[®], M. H. Liu[®], Q. Y. Liu[®], Z. Q. Liu[®], D. Liventsev[®], S. Longo[®], T. Lueck[®], C. Lyu[®], Y. Ma[®], M. Maggiora[®], S. P. Maharana[®], R. Maiti[®], S. Maity[®], G. Mancinelli[®], R. Manfredi[®], E. Manoni[®], M. Mantovano[®], D. Marcantonio, S. Marcello, C. Marina, C. Martellini, A. Martens, A. Martini, T. Martino, T. Martinov, L. Massaccesi, M. Masuda[®], K. Matsuoka[®], D. Matvienko[®], S. K. Maurya[®], J. A. McKenna[®], F. Meier[®], M. Merola[®], F. Metzner[®], C. Miller, M. Mirra, S. Mitra, K. Miyabayashi, G. B. Mohanty, S. Mondal, S. Moneta, H.-G. Moser, M. Mrvar, I. Nakamura, M. Nakao, Y. Nakazawa, M. Naruki, D. Narwal, Z. Natkaniec, A. Natochii, M. Nayak, G. Nazaryan, M. Neu, M. Niiyama, S. Nishida, S. Ogawa, Y. Onishchuk, H. Ono, G. Pakhlova, S. Pardi[®], K. Parham[®], H. Park[®], J. Park[®], S.-H. Park[®], B. Paschen[®], A. Passeri[®], S. Patra[®], S. Paul[®], T. K. Pedlar[®], R. Peschke[®], R. Pestotnik[®], M. Piccolo[®], L. E. Piilonen[®], G. Pinna Angioni[®], P. L. M. Podesta-Lerma[®], T. Podobnik[®], S. Pokharel[®], C. Praz[®], S. Prell[®], E. Prencipe[®], M. T. Prim[®], I. Prudiiev[®], H. Purwar[®], P. Rados[®], G. Raeuber[®], S. Raiz[®], N. Rauls[®], M. Reif[®], S. Reiter[®], M. Remnev[®], L. Reuter[®], I. Ripp-Baudot[®], G. Rizzo[®], S. H. Robertson[®], M. Roehrken, J. M. Roney, A. Rostomyan, N. Rout, S. Sandilya, L. Santelj, Y. Sato, V. Savinov, B. Scavino, S. Schneider, G. Schneil, M. Schnep, K. Schoenning, C. Schwand, Y. Seino, A. Selce, K. Senyo, J. Serrano, M. E. Sevior, C. Sfienti, W. Shan, C. Sharma, C. P. Shen, X. D. Shi, T. Shillington, T. Shimasaki, J.-G. Shiu, D. Shtol, A. Sibidanov, F. Simon, J. B. Singh, J. Skorupa, R. J. Sobie, M. Sobotzik[®], A. Soffer[®], A. Sokolov[®], E. Solovieva[®], S. Spataro[®], B. Spruck[®], M. Starič[®], P. Stavroulakis[®], S. Stefkova[®], R. Stroili[®], Y. Sue[®], M. Sumihama[®], N. Suwonjandee[®], H. Svidras[®], M. Takizawa[®], U. Tamponi[®], K. Tanida, F. Tenchini, A. Thaller, O. Tittel, R. Tiwary, D. Tonelli, E. Torassa, K. Trabelsi, I. Ueda, T. Uglov[®], K. Unger[®], Y. Unno[®], K. Uno[®], S. Uno[®], Y. Ushiroda[®], S. E. Vahsen[®], R. van Tonder[®], K. E. Varvell[®], M. Veronesi[®], A. Vinokurova[®], V. S. Vismaya[®], L. Vitale[®], V. Vobbilisetti[®], R. Volpe[®], A. Vossen[®], B. Wach[®], M. Wakai, S. Wallner, E. Wang, M.-Z. Wang, X. L. Wang, Z. Wang, A. Warburton, S. Watanuki, C. Wessel[®], E. Won[®], Y. Xie[®], X. P. Xu[®], B. D. Yabsley[®], S. Yamada[®], W. Yan[®], S. B. Yang[®], J. Yelton[®], J. H. Yin[®], Y. M. Yook[®], K. Yoshihara[®], C. Z. Yuan[®], Y. Yusa[®], L. Zani[®], F. Zeng[®], B. Zhang[®], V. Zhilich[®], J. S. Zhou[®], O. D. Zhou, V. I. Zhukova, and R. Žlebčík

(Belle and Belle II Collaborations)

(Received 1 June 2024; accepted 11 July 2024; published 26 August 2024)

We report the result of a search for the rare decay $B^0 \to \gamma \gamma$ using a combined dataset of $753 \times 10^6 \ B\bar{B}$ pairs collected by the Belle experiment and $387 \times 10^6 \ B\bar{B}$ pairs collected by the Belle II experiment from decays of the $\Upsilon(4S)$ resonance produced in e^+e^- collisions. A simultaneous fit to the Belle and Belle II data sets yields $11.0^{+6.5}_{-5.5}$ signal events, corresponding to a 2.5σ significance. We determine the branching fraction $\mathcal{B}(B^0 \to \gamma \gamma) = (3.7^{+2.2}_{-1.8}(\text{stat}) \pm 0.5(\text{syst})) \times 10^{-8}$ and set a 90% credibility level upper limit of $\mathcal{B}(B^0 \to \gamma \gamma) < 6.4 \times 10^{-8}$.

DOI: 10.1103/PhysRevD.110.L031106

In the standard model (SM), there is no tree-level interaction between the b quark and the d quark; therefore, the $B^0 \rightarrow \gamma \gamma$ proceeds through a flavor changing neutral current transition involving electroweak loop amplitudes where a quark emits and reabsorbs a W^- gauge boson. The dominant amplitudes are illustrated in Fig. 1.

The charge-conjugation and parity (CP) averaged branching fraction $\mathcal{B}(B^0 \to \gamma \gamma)$ is predicted in the SM to be $(1.4^{+1.4}_{-0.8}) \times 10^{-8}$, including next-to-leading logarithmic and next-to-leading power corrections [1]. Although the long-distance penguin contribution is expected to be negligible, it can noticeably impact the CP-violating observables [2]. The decay $B^0 \to \gamma \gamma$ is sensitive to physics beyond the SM since contributions of non-SM particles in the loop could enhance the branching fraction by an order of magnitude to a few orders of magnitude above the SM expectation, depending on specific supersymmetric parameter values [3,4]. A measurement of $B^0 \to \gamma \gamma$ thus offers an attractive opportunity to test theories beyond the SM [3–5].

The most stringent upper limit (UL) on the branching fraction is $\mathcal{B}(B^0 \to \gamma \gamma) < 3.2 \times 10^{-7}$ at the 90% confidence level (CL), set by the BABAR experiment [6] using an $e^+e^$ dataset recorded at the $\Upsilon(4S)$ resonance with an integrated luminosity of 426 fb⁻¹. The Belle experiment obtained the upper limit $\mathcal{B}(B^0 \to \gamma \gamma) < 6.2 \times 10^{-7}$ at the 90% CL with a 104 fb⁻¹ e^+e^- dataset from the $\Upsilon(4S)$ [7].

Here, we report a search for the decay $B^0 \rightarrow \gamma \gamma$ using a combined e^+e^- dataset from the Belle and Belle II experiments collected at the $\Upsilon(4S)$ resonance energy. For Belle, we use a dataset corresponding to 694 fb⁻¹ containing $(753 \pm 10) \times 10^6 \ B\bar{B}$ pairs, while for Belle II we use 362 fb⁻¹ collected between 2019 and 2022, corresponding to $(387 \pm 6) \times 10^6 \ B\bar{B}$ pairs. The number of $B\bar{B}$ events from Belle used in this analysis is slightly smaller than that of the entire Belle dataset $(772 \pm 11) \times 10^6$, as we only use

Published by the American Physical Society under the terms of the Creative Commons Attribution 4.0 International license. Further distribution of this work must maintain attribution to the author(s) and the published article's title, journal citation, and DOI. Funded by SCOAP³.

the data containing calorimeter timing information. The analysis does not distinguish between B^0 and \bar{B}^0 , and throughout this article, charge conjugation is implied for all decays.

The Belle detector was a cylindrical large-solid-angle magnetic spectrometer located at the interaction point of the KEKB asymmetric energy e^+e^- collider [8]. The detector consisted of a silicon vertex detector, a central drift chamber, an array of aerogel threshold Cherenkov counters, a barrel-like arrangement of time-of-flight scintillation counters, and an electromagnetic calorimeter (ECL) composed of CsI(Tl) crystals located inside a super-conducting solenoid coil that provided a 1.5 T axial magnetic field. An iron flux-return located outside the coil was instrumented to detect K_L^0 mesons and to identify muons. A detailed description of the detector can be found in Ref. [9].

The Belle II detector [10], located at the SuperKEKB e^+e^- collider [11], is an upgraded version of the Belle detector. Belle II includes a silicon vertex detector consisting of pixel sensors and double-sided strip detectors, and a central drift chamber. The central drift chamber is surrounded by two types of Cherenkov light detector systems: time-of-propagation detectors for the barrel region and an aerogel ring-imaging Cherenkov detector for the forward end cap region. The Belle ECL is reused in Belle II along with the solenoid and the iron flux return voke. However, the ECL readout electronics has been upgraded [10]. The solenoid flux return is instrumented with resistive-plate chambers and plastic scintillator mod-

ules to detect muons, K_L^0 mesons, and neutrons. The z axis of the laboratory frame is defined as the solenoid axis, where the positive direction is approximately

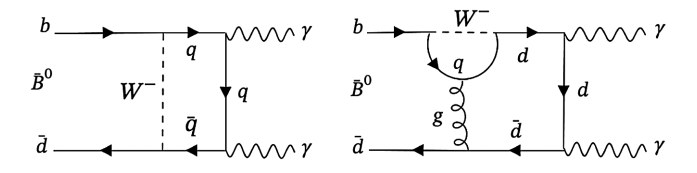


FIG. 1. Box (left) and penguin (right) amplitudes contributing to $\bar{B}^0 \to \gamma \gamma$ at leading order in the SM. The symbol q represents a u, c, or t quark.

that of the electron beam. This convention applies both to Belle and Belle II.

Monte Carlo simulated events are used to optimize the selection criteria, estimate signal selection efficiencies, train multivariate discriminants, identify various sources of background, and develop a model to fit data. We examine the data after all the requirements are fixed to avoid experimenter's bias. To study the signal, we use 10⁵ $\Upsilon(4S) \to B^0 \bar{B}^0$ simulated decays in which one B^0 meson decays as $B^0 \rightarrow \gamma \gamma$ and the other decays according to known decay modes tabulated by the Particle Data Group [12]. The simulated signal and $e^+e^- \rightarrow B\bar{B}$ samples are generated using the EvtGen [13] and PYTHIA 8.2 [14] software packages, and the detector response is simulated using Geant3 [15] and Geant4 [16] for Belle and Belle II, respectively. Continuum $e^+e^- \rightarrow q\bar{q}$ background processes, where q = u, d, s, c are generated by PYTHIA 6.4 for Belle [17]. In the case of Belle II, the KKMC [18] generator is used for hard scattering, followed by PYTHIA 8.2 [14] for the hadronization process. In addition, a sample of $e^+e^- \rightarrow \tau^+\tau^-$ events is generated with the TAUOLA package [19]. The simulated samples of the aforementioned background events corresponding to 1 ab⁻¹ or more are used. To validate the simulations of continuum processes, Belle (Belle II) has collected 89.5 (42.3) fb⁻¹ of data about 60 MeV below the $\Upsilon(4S)$ peak. Experimental and simulated Belle data are converted into Belle II format [20] and processed with the Belle II software [21,22].

Candidate $B^0 \rightarrow \gamma \gamma$ decays are characterized by two nearly back-to-back highly energetic photons in the $e^+e^$ center-of-mass (c.m.) frame, as B^0 mesons are produced almost at rest. Photons are selected from isolated energy deposits (clusters) in the ECL that are not associated with charged particle trajectories (tracks). We select events containing at least two photons with energies in the range $1.4 < E^*(\gamma) < 3.4 \text{ GeV}$, where the asterisk denotes an observable in the e^+e^- c.m. frame. Only ECL clusters with polar angle θ in the 33° < θ < 132° barrel region are considered. To reject background from merged photon clusters and neutral hadrons, we require that $E_9/E_{25}(E_9/E_{21}) > 0.95$ for Belle (Belle II). In Belle, E_9/E_{25} corresponds to the ratio of energy deposits between (3×3) and (5×5) crystals centered on the crystal with maximum energy, whereas in Belle II, E_{21} corresponds to the energy of the (5×5) crystals, excluding the corners. To suppress clusters originating from neutral hadrons, the number of crystals with energy above 20 MeV in the clusters must exceed 15. To distinguish between photon and K_{I}^{0} showers, we utilize a boosted decision tree (BDT) [23] trained using Zernike moments [24] as inputs. The classifier output must have a value above 0.75, which is 90% efficient in selecting the signal while rejecting 74% of the background events. To reject out-of-time QED processes such as Bhabha scattering or $e^+e^- \rightarrow \gamma\gamma$, the ECL cluster hit time is required to be within a $2~\mu s$ window around the beam crossing time. For Belle II, the photon signal time, calculated from the fitted time of the highest energy crystal's recorded waveform within the cluster, should not differ from the beam crossing time by more than 200~ns.

The $B^0 \to \gamma \gamma$ signal candidates are reconstructed by combining two photon candidates and selected using the beam-constrained mass $M_{\rm bc}$ and energy difference ΔE defined as

$$M_{\rm bc} = \sqrt{(E_{\rm beam}^*/c^2)^2 - (p_{B^0}^*/c)^2},$$
 (1)

$$\Delta E = E_{p0}^* - E_{\text{beam}}^*, \tag{2}$$

where $E_{\rm beam}^*$ is the beam energy, $E_{B^0}^*$ and $p_{B^0}^*$ are the energy and momentum of the B^0 candidate, all calculated in the e^+e^- c.m. frame. The signal events peak at the B^0 meson mass in the $M_{\rm bc}$ distribution and concentrate near zero in the ΔE distribution. Hence, the B^0 meson candidates are required to be in the range $5.24 < M_{\rm bc} < 5.29~{\rm GeV}/c^2$ and $-0.6 < \Delta E < 0.2~{\rm GeV}$. The ΔE window is not centered around zero because of energy leakage from the ECL. No events with multiple B^0 candidates are found in the experimental or simulated signal data. To reduce $e^+e^- \to q\bar{q}$ and $\tau^+\tau^-$ events, we require at least three tracks in the event and the ratio of the second and zeroth Fox Wolfram moments [25] to be less than 0.7. This ratio is computed using the momenta of all charged and neutral particles within the event.

To suppress the background from asymmetric-energy decays of $\pi^0 \to \gamma \gamma$ and $\eta \to \gamma \gamma$ decays, a π^0/η veto is implemented. The initial step is to pair each high-energy photon candidate with low-energy photon candidates having energies above 50 MeV in the event. The probability of a correctly reconstructed π^0/η is then obtained using a BDT (BDT_{veto}) trained on a dedicated sample dominated by π^0 and η events. For training, we use a set of variables characterizing the photon pairs, including their invariant mass, the cosine of the angle in the π^0/η rest frame between the momentum of the high-energy photon and the boost direction of π^0/η from the laboratory frame. Other variables for the low-energy photon include its energy, its polar angle, the total number of crystal hits in the ECL, and the cluster variable $E_9/E_{21(25)}$. For Belle II, we use two additional variables: the distance between the ECL cluster and the nearest charged particle trajectory extrapolated to the ECL, and the output of a multivariate classifier based on Zernike moments for the low-energy photon. All the selection criteria described above are optimized by maximizing $\varepsilon_{\rm sig}/(3/2+\sqrt{\rm B})$ [26], where $\varepsilon_{\rm sig}$ is the efficiency of the event selection calculated from $B^0 \rightarrow \gamma \gamma$ simulation, and B is the expected number of background events in the signal region. The optimized BDT_{veto} selection in Belle rejects 78% of background photons from π^0/η decays while retaining 85% of the signal. Similarly, the Belle II selection rejects 75% of this background while retaining 82% of the signal.

The dominant source of the remaining background is from the continuum. Since light quarks carry significant momenta, continuum events are jetlike and are therefore topologically different from isotropic $B^0\bar{B}^0$ events in which B^0 meson pairs are produced nearly at rest in the c.m. frame. These differences in event shape topology provide most of the discrimination against continuum background. We separately train a BDT_{$q\bar{q}$} classifier using 21 variables for both Belle and Belle II data. The classification is based on modified Fox-Wolfram moments [25], the cosine of the angle between the thrust axis of the B^0 meson and the z axis, the cosine of the angle between the thrust axis of the signal B^0 candidate and the thrust axis of the rest of the event (the other B^0 in a correctly reconstructed event) [27]. the cosine of the angle between the B^0 flight direction and the z-axis, the number of tracks in the event, and the flavor tagger output [28], which determines the flavor of the tag (non-signal) side B^0 meson. If the flavor tagger fails to find a tag for a B^0 candidate, which is generally the case for continuum background, the absence of B^0 -flavor information is noted and input to $BDT_{q\bar{q}}$.

The BDT output, $C_{\mathrm{BDT}_{q\bar{q}}}$, ranges from 0 to 1, with a value near 1(0) being more likely for a signal (background) event. We use simulated samples to determine a minimum threshold on the continuum classifier output that minimizes the average expected statistical uncertainty of the signal yield. This selection requires $C_{\mathrm{BDT}_{q\bar{q}}} > 0.55$ ($C_{\mathrm{BDT}_{q\bar{q}}} > 0.45$), which rejects 93% (87%) of the $q\bar{q}$ background and retains 86% (89%) of the signal when applied to the Belle (Belle II) simulation. After applying all the selection criteria, the overall signal reconstruction efficiency for Belle and Belle II is $(23.3 \pm 0.1)\%$ and $(30.8 \pm 0.1)\%$, respectively, where the uncertainties are statistical.

In addition, we evaluate the impact of $B^0 \to \pi^0 \pi^0$, $B^0 \to \eta \eta$, $B^0 \to \eta \pi^0$, and $B^0 \to \omega \gamma$ background events. The largest contribution, from $B^0 \to \pi^0 \pi^0$ decay, constitutes 0.03 events. Therefore, we conclude these rare B decay backgrounds are negligible.

To extract the signal yield, we perform a three-dimensional extended unbinned maximum likelihood fit to $M_{\rm bc}$, ΔE , and $C'_{\rm BDT}$, where $C'_{\rm BDT}$ is the output of the BDT ($C_{\rm BDT_{q\bar{q}}}$) transformed using the probability integral transformation [29]. The $C'_{\rm BDT}$ distribution for the simulated signal is uniform between zero and one, whereas the background distribution exhibits a peak at zero, simplifying modeling. The likelihood function is defined as

$$\mathcal{L}_{\text{fit}} = e^{-\sum_{j} n_{j}} \prod_{i}^{N} \left(\sum_{j} n_{j} P_{j}((M_{\text{bc}})^{i}, (\Delta E)^{i}, (C'_{\text{BDT}})^{i}) \right), \quad (3)$$

where P_i $(M_{bc}, \Delta E, C'_{BDT})$ is the probability density function (PDF) of the signal or background component (specified by index j), n_i is the yield of this component, i represents the event index, and N is the total number of events in the sample. The PDFs for the signal and background are based on simulation. To model the $M_{\rm bc}$ and ΔE signal distribution, a two-dimensional kernel-density [30] shape is employed to account for the correlation between $M_{\rm bc}$ and ΔE , which is 26% and 17% for Belle and Belle II, respectively. The distribution of C'_{BDT} for the signal is modeled by a constant function. The background is characterized by an ARGUS function [31] for the $M_{\rm bc}$ distribution, while the ΔE distribution is modeled using a first-order Chebychev polynomial. The C'_{BDT} distribution is modeled by a sum of two exponential functions. All the signal parameters, C'_{BDT} background parameters, and the ARGUS endpoint are fixed to the best-fit values obtained from one-dimensional fits to simulated events. All other background shape parameters and the signal and background yields are allowed to vary in the fit.

To test for bias in the fitted signal yield, we perform ensemble tests for Belle and Belle II for different signal yields. Signal events are randomly selected from simulation, while the expected number of background events are generated from the nominal PDFs. Statistical fluctuations in the number of signal and background events are included, assuming that the events follow Poisson statistics. Each simulated experiment is repeated 1000 times for signal yield ranging from 2 to 20 events and fitted with the nominal model as defined in Eq. (3). The average deviation between the fitted and generated signal yields is treated as a source of systematic uncertainty. Additionally, we include the linearity of fit results relative to signal yield as an additional source of systematic uncertainty. Combined in quadrature, this yields a +0.14 (+0.10) uncertainty on the fit bias for Belle (Belle II).

The systematic uncertainty associated with fixing the parameter values of the PDFs is assessed by varying the best-fit parameter values within $\pm 1\sigma$ of their statistical uncertainties. The resulting deviations in the signal yields in data are measured and used to quantify this uncertainty. A systematic uncertainty of $^{+0.56}_{-0.48}$ (($^{+0.28}_{-0.32}$)) events is assigned to the fit model for Belle (Belle II). To evaluate the accuracy of the simulation in describing data distributions, we compare its predictions to data from a $B^0 \to K^*(892)^0 \gamma$ control sample. The $K^*(892)^0$ mesons are reconstructed using $K^*(892)^0 \to K^+\pi^-$ decays, in which the charged kaon is required to have $R_{K/\pi} = \mathcal{L}_K/(\mathcal{L}_K + \mathcal{L}_\pi) > 0.6$, where $\mathcal{L}_{K(\pi)}$ is the likelihood for the kaon(pion) hypothesis, which combines information from various subdetectors of Belle or Belle II. The photon selection criteria are the same as in the signal reconstruction. In addition, the invariant mass of the $K^+\pi^-$ meson pair should be in the range $0.817 < M_{K^*} < 0.968 \text{ GeV}/c^2$. The deviations from unity

TABLE I. Summary of additive systematic uncertainties.

Source	Belle (events)	Belle II (events)	Combined (events)
Fit bias	+0.14	+0.10	+0.12
PDF parametrization	$+0.56 \\ -0.48$	+0.28 -0.32	+0.52 -0.44
Shape modeling	+0.06	+0.04	+0.05
Total (sum in quadrature)	$^{+0.58}_{-0.48}$	$^{+0.30}_{-0.32}$	$+0.54 \\ -0.44$

in the data/MC ratio for the distributions of $M_{\rm bc}$ and ΔE are considered as a source of systematic uncertainty. By adding them in quadrature, we assign a systematic uncertainty of +0.06 (+0.04) events for Belle (Belle II) as the signal shape uncertainty. These uncertainties are combined in quadrature, resulting in a systematic uncertainty of $^{+0.58}_{-0.48}$ $\binom{+0.30}{-0.32}$ events, as presented in Table I. These uncertainties are treated as additive systematic uncertainties that affect the significance of the observed signal yield. Table II includes uncertainties in the photon detection efficiency, the signal reconstruction efficiency, the number of produced $B\bar{B}$ pairs, and the branching fraction of $\Upsilon(4S)$ to neutral $B\bar{B}$ pairs, f^{00} [32]. These uncertainties are multiplicative, which are proportional to the signal yield and affect the signal efficiency in the denominator of Eq. (4). The systematic uncertainty arising from the photon detection efficiency is determined to be 4.0% for Belle using the recoil technique in $e^+e^- \rightarrow e^+e^-\gamma$ radiative Bhabha events. For Belle II data, it is measured to be 2.7% utilizing a $e^+e^- \rightarrow \mu^+\mu^-\gamma$ initial-state radiation data sample. The uncertainty in signal reconstruction efficiency is due to the limited size of the signal simulated sample, and is determined to be 0.4% (0.3%) for Belle (Belle II). The uncertainties on the number of $B\bar{B}$ pairs recorded in Belle and Belle II are also considered. A systematic uncertainty from the efficiency of the requirement on C_{BDT} and the π^0/η veto is estimated using the $B^0 \to K^*(892)^0 \gamma$ control sample. The efficiency ratio between the data and simulation of those requirements is used as correction, and its uncertainty as the associated systematic error. Since there

TABLE II. Summary of multiplicative systematic uncertainties.

Source	Belle (%)	Belle II (%)	Combined (%)
Photon detection efficiency	4.0	2.7	3.5
Simulation sample size	0.4	0.3	0.3
Number of $B\bar{B}$	1.3	1.5	1.0
f^{00}	2.5	2.5	2.5
C_{BDT} requirement	0.4	0.9	0.6
π^0/η veto	0.4	0.6	0.4
Timing requirement efficiency	2.8	•••	2.7
Total (sum in quadrature)	5.7	4.1	5.2

are two photons in the final state for signal candidates and only one in the control mode, the correction and systematic uncertainty are doubled. The efficiency ratio between the data and simulation due to the $C_{\rm BDT}$ and the π^0/η veto requirements for Belle (Belle II) are 1.026 ± 0.004 (1.006 ± 0.009) and 1.004 ± 0.004 (1.002 ± 0.006), respectively. An uncertainty of 2.8% is assigned due to the timing criteria for Belle, while for Belle II, the uncertainty is incorporated into the photon detection efficiency.

We obtain $9.1^{+5.6}_{-4.4}$ ($1.9^{+4.2}_{-2.8}$) signal events and 615 ± 25 (317 ± 18) background events for Belle (Belle II) from the fits to the two independent datasets. The branching fraction is calculated using the equation

$$\mathcal{B}(B^0 \to \gamma \gamma) = \frac{N_{\text{sig}}^{\text{fit}}}{2 \times N_{B\bar{B}} \times \epsilon_{\text{rec}} \times f^{00}}, \tag{4}$$

where $N_{\rm sig}^{\rm fit}$ represents the signal yield obtained from the fit, $N_{B\bar{B}}=(753\pm10)\times10^6$ and $(387\pm6)\times10^6$ is the number of $B\bar{B}$ pairs at the $\Upsilon(4{\rm S})$ resonance for Belle and Belle II, $\epsilon_{\rm rec}=23.3\%$ and 30.8% are the signal reconstruction efficiencies for Belle and Belle II, respectively, and $f^{00}=(48.4\pm1.2)\%$. Therefore, the branching fractions for the Belle and Belle II datasets are $(5.4^{+3.3}_{-2.6}\pm0.5)\times10^{-8}$ and $(1.7^{+3.7}_{-2.4}\pm0.3)\times10^{-8}$, respectively. The first uncertainty is statistical, while the second is systematic.

In addition, we perform an extended unbinned maximum likelihood fit to the $M_{\rm bc}$, ΔE , and $C'_{\rm BDT}$ distributions simultaneously in the Belle and Belle II datasets, which is shown in Fig. 2. The branching fraction is determined to be $(3.7^{+2.2}_{-1.8}\pm 0.5)\times 10^{-8}$ with a total signal (background) yield of $11.0^{+6.5}_{-5.5}$ (931 ± 31) events, where the uncertainties are statistical only. The combined systematic uncertainty is calculated as the maximum deviation between the fitted values and the best-fit values with the inclusion of systematic uncertainty in the simultaneous fit. The signal significance is calculated as $\sqrt{-2\ln(\mathcal{L}_0/\mathcal{L}_{\text{max}})}$, where \mathcal{L}_0 is the maximum value of the likelihood when signal yield is fixed to zero, and \mathcal{L}_{max} is the maximum value of the likelihood of the nominal fit. The resulting significance is 2.5σ , which includes the systematic uncertainties. To include systematic uncertainties in the significance, we convolve the likelihood distribution with a Gaussian function whose width is set to the total systematic uncertainty.

As the significance of the signal yield is low, we calculate an upper limit (UL) on the \mathcal{B} using a Bayesian approach, with a flat prior. The UL on the branching fraction is determined by integrating the likelihood function including the systematic uncertainty from zero to 90% of the area under the curve. The upper limit on the branching fraction obtained from the combined dataset is 6.4×10^{-8} , at 90% credibility level [33]. The expected upper limit from the simulation is 4.4×10^{-8} at 90% credibility level.

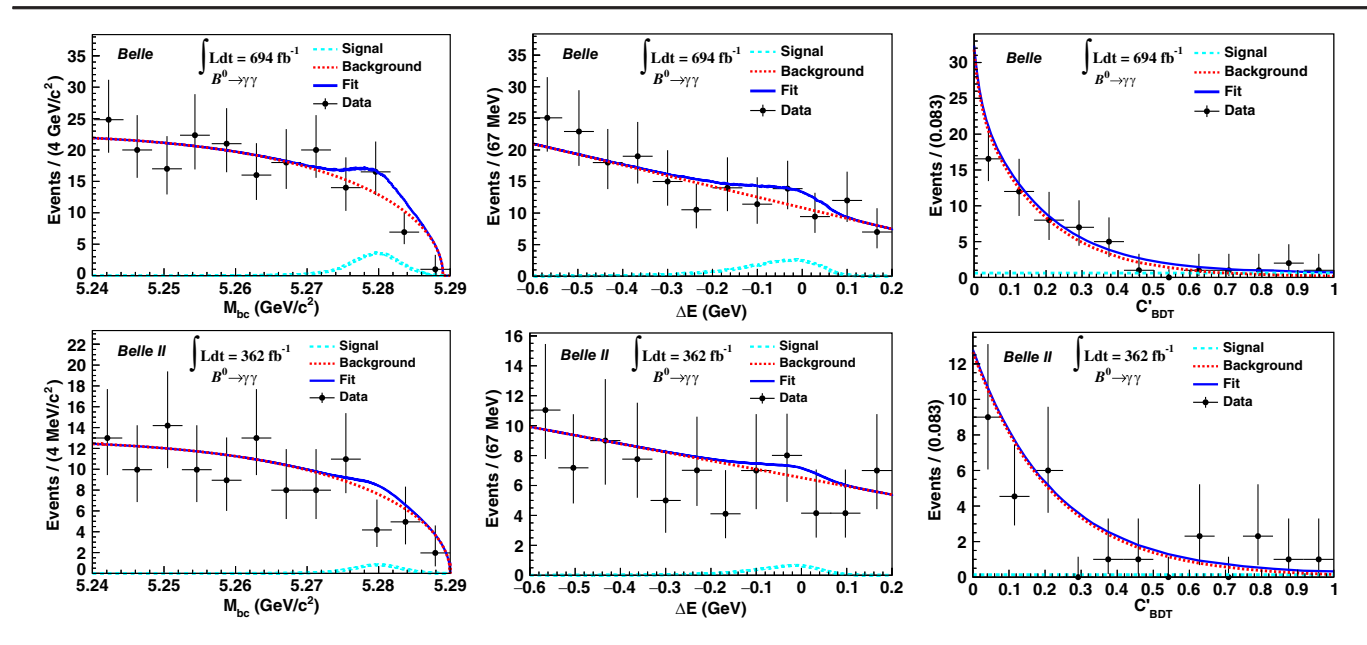


FIG. 2. Signal enhanced projections of $M_{\rm bc}$ (left), ΔE (middle), and $C'_{\rm BDT}$ (right) for the $B^0 \to \gamma \gamma$ analysis using the Belle (top) and Belle II (bottom) dataset. For each plot, we apply the signal region selection criteria on the variables other than the plotted variable. The signal regions for the first two variables are as follows, $5.27 < M_{\rm bc} < 5.29~{\rm GeV}/c^2$ and $-0.19 < \Delta E < 0.14~{\rm GeV}$ for Belle and $5.27 < M_{\rm bc} < 5.29~{\rm GeV}/c^2$ and $-0.19~{\rm GeV} < \Delta E < 0.15~{\rm GeV}$ for Belle II. The cyan (dashed), red (dotted), and blue (solid) color distributions represent the signal, continuum background, and total fit function, respectively. Points with error bars represent data.

The measured branching fractions and the resulting upper limits on $\mathcal{B}(B^0 \to \gamma \gamma)$ at 90% credibility level, including the systematic uncertainties, are summarized in Table III.

In summary, we have searched for the decay $B^0 \rightarrow \gamma \gamma$ using a 1.1 ab⁻¹ data sample collected at the $\Upsilon(4S)$ resonance by the Belle and Belle II experiments. No statistically significant signal is observed, leading us to set an upper limit of 6.4×10^{-8} on the branching fraction at 90% credibility level. This result supersedes the previous Belle measurement [7] and represents a significant improvement over the previous searches by the BABAR and Belle collaborations. The use of advanced analysis techniques such as BDTs results in a factor of two background reduction compared to the BABAR results and a gain of a factor of two in the signal reconstruction efficiency compared to the previous Belle measurements. These improvements, combined with the larger Belle + Belle II dataset, lead to an UL that is five times more restrictive than the previous best limit from BABAR [6].

TABLE III. Summary of $\mathcal{B}(B^0 \to \gamma \gamma)$ measurements and UL's at 90% credibility level.

	$\mathcal{B}(B^0 o \gamma \gamma)$	UL on $\mathcal{B}(B^0 \to \gamma \gamma)$
Belle	$(5.4^{+3.3}_{-2.6} \pm 0.5) \times 10^{-8}$	$<9.9 \times 10^{-8}$
Belle II	$(1.7^{+3.7}_{-2.4} \pm 0.3) \times 10^{-8}$	$< 7.4 \times 10^{-8}$
Combined	$(3.7^{+2.2}_{-1.8} \pm 0.5) \times 10^{-8}$	$< 6.4 \times 10^{-8}$

This work, based on data collected using the Belle II detector, which was built and commissioned prior to March 2019, and data collected using the Belle detector, which was operated until June 2010, was supported by Higher Education and Science Committee of the Republic of Armenia Grant No. 23LCG-1C011; Australian Research and Research Grants No. DP200101792, Council No. DP210101900, No. DP210102831, No. DE220100462, No. LE210100098, LE230100085; Austrian Federal No. Ministry Education, Science and Research, Austrian Science Fund No. P 34529, No. J 4731, No. J 4625, and No. M 3153, and Horizon 2020 ERC Starting Grant No. 947006 "InterLeptons"; Natural Sciences and Engineering Research Council of Canada, Compute Canada and CANARIE; National Key R&D Program of China under Contract No. 2022YFA1601903, National Natural Science Foundation of China and Research Grants No. 11575017, No. 11761141009, No. 11705209, No. 11975076, No. 12135005, No. 12150004, No. 12161141008, and No. 12175041, and Shandong Provincial Natural Science Foundation Project ZR2022JQ02; the Czech Science Foundation Grant No. 22-18469S and Charles University Grant Agency project No. 246122; European Research Council, Seventh Framework PIEF-GA-2013-622527, Horizon 2020 ERC-Advanced Grants No. 267104 and No. 884719, Horizon 2020 ERC-Consolidator Grant No. 819127, Horizon 2020 Marie Sklodowska-Curie Grant Agreement No. 700525 "NIOBE" and No. 101026516, and Horizon 2020 Marie Sklodowska-Curie RISE project JENNIFER2 Grant Agreement No. 822070 (European grants); L'Institut National de Physique Nucléaire et de Physique des Particules (IN2P3) du CNRS and L'Agence Nationale de la Recherche (ANR) under Grant ANR-21-CE31-0009 (France); BMBF, DFG, HGF, MPG, and AvH Foundation (Germany); Department of Atomic Energy under Project Identification No. RTI 4002, Department of Science and Technology, and UPES SEED funding Programs UPES/R&D-SEED-INFRA/17052023/01 No. No. UPES/R&D-SOE/20062022/06 (India); Israel Science Foundation Grant No. 2476/17, U.S.-Israel Binational Science Foundation Grant No. 2016113, and Israel Ministry of Science Grant No. 3-16543; Istituto Nazionale di Fisica Nucleare and the Research Grants BELLE2; Japan Society for the Promotion of Science, Grant-in-Aid for Scientific Research Grants No. 16H03968, No. 16H03993, No. 16H06492, No. 16K05323, No. 17H01133, No. 17H05405. No. 18K03621. No. 18H03710. 20H05850, No. 18H05226, No. 19H00682, No. No. 20H05858, No. 22H00144, No. 22K14056, No. 22K21347, No. 23H05433, No. 26220706, and No. 26400255, and the Ministry of Education, Culture, Sports, Science, and Technology (MEXT) of Japan; National Research Foundation (NRF) of Korea Grants No. 2016R1D1A1B02012900, No. 2018R1A2B3003643, 2018R1A6A1A06024970, No. 2019R1I1A3 A01058933, No. 2021R1A6A1A03043957, No. 2021R1F1 A1060423, No. 2021R1F1A1064008, No. 2022R1A2 C1003993, and No. RS-2022-00197659, Radiation Science Research Institute, Foreign Large-Size Research Facility Application Supporting project, the Global Science Experimental Data Hub Center of the Korea Institute of Science and Technology Information and KREONET/Global Ring Network for Advanced Application Development (GLORIAD); Universiti Malaya RU grant, Akademi Sains Malaysia, and Ministry of Education Malaysia; Frontiers of Science Program Contracts No. FOINS-296, No. CB-221329, No. CB-236394, No. CB-254409, and No. CB-180023, and SEP-CINVESTAV Research Grant No. 237 (Mexico); the Polish Ministry of Science and Higher Education and the National Science Center; the Ministry of Science and Higher Education of the Russian Federation and the HSE University Basic Research Program, Moscow; University of Tabuk Research Grants No. S-0256-1438 and No. S-0280-1439 (Saudi Arabia); Slovenian Research Agency and Research Grants No. J1-9124 and No. P1-0135; Ikerbasque, Basque Foundation for Science, the State Agency for Research of the Spanish Ministry of Science and Innovation through Grant No. PID2022-136510NB-C33, Agencia Estatal de Investigacion, Spain Grant No. RYC2020-029875-I and Generalitat Valenciana, Spain Grant No. CIDEGENT/2018/020; the Swiss National Science Foundation; The Knut and Alice Wallenberg Foundation (Sweden), Contracts No. 2021.0174 and No. 2021.0299; National Science and Technology Council, and Ministry of Education (Taiwan); Thailand Center of Excellence in Physics; TUBITAK ULAKBIM (Turkey); National Research Foundation of Ukraine, Project No. 2020.02/0257, and Ministry of Education and Science of Ukraine; the U.S. National Science Foundation and Research Grants No. PHY-1913789 and No. PHY-2111604, and the U.S. Department of Energy and Research Awards No. DE-AC06-76RLO1830, No. DE-SC0007983, No. DE-SC0009824, No. DE-SC0009973, No. DE-SC0010007, No. DE-SC0010073, No. DE-SC0010118, No. DE-SC0010504, No. DE-SC0011784, No. DE-SC0012704, No. DE-SC0019230, No. DE-SC0021274, No. DE-SC0021616, No. DE-SC0022350, No. DE-SC0023470; and the Vietnam Academy of Science and Technology (VAST) under Grants No. NVCC.05.12/22-23 and No. DL0000.02/24-25. These acknowledgements are not to be interpreted as an endorsement of any statement made by any of our institutes, funding agencies, governments, or their representatives. We thank the SuperKEKB team for delivering high-luminosity collisions; the KEK cryogenics group for the efficient operation of the detector solenoid magnet; the KEK Computer Research Center for on-site computing support; the NII for Science Information NETwork 6 (SINET6) network support; and the raw-data centers hosted by BNL, DESY, GridKa, IN2P3, INFN, PNNL/EMSL, and the University of Victoria.

^[1] Y.-L. Shen, Y.-M. Wang, and Y.-B. Wei, J. High Energy Phys. 12 (2020) 169.

^[2] Qin Qin, Y.-L. Shen, C. Wang, and Y.-M. Wang, Phys. Rev. Lett. **131**, 091902 (2023).

^[3] G. G. Devidze and G. R. Jibuti, Phys. Lett. B 429, 48 (1998).

^[4] G. Devidze, A. Liparteliani, and Ulf-G. Meißner, Phys. Lett. B **634**, 59 (2006).

^[5] J. I. Aranda, J Montano, F. Ramirez-Zavaleta, J. J. Toscano, and E. S. Tututi, Phys. Rev. D 82, 054002 (2010).

^[6] P. del Amo Sanchez *et al.* (*BABAR* Collaboration), Phys. Rev. D **83**, 032006 (2011).

^[7] S. Villa *et al.* (Belle Collaboration), Phys. Rev. D 73, 051107 (2006).

^[8] S. Kurokawa and E. Kikutani, Nucl. Instrum. Methods Phys. Res., Sect. A **499**, 1 (2003); T. Abe *et al.*, Prog. Theor. Exp. Phys. **2013**, 03A001 (2013), and references therein.

^[9] A. Abashian *et al.* (Belle Collaboration), Nucl. Instrum. Methods Phys. Res., Sect. A **479**, 117 (2002).

- [10] T. Abe *et al.* (Belle II Collaboration), KEK Report No. 2010-1, 2010, arXiv:1011.0352.
- [11] A. Kazunori, F. Kazuro, K. Haruyo (SuperKEKB Accelerator Team), Nucl. Instrum. Methods Phys. Res., Sect. A 907, 188 (2018).
- [12] R. L. Workman *et al.* (Particle Data Group), Prog. Theor. Exp. Phys. **2022**, 083C01 (2022).
- [13] D. J. Lange, Nucl. Instrum. Methods Phys. Res., Sect. A 462, 152 (2001).
- [14] T. Sjostrand et al., Comput. Phys. Commun. 191, 159 (2015).
- [15] R. Brun et al., Geant 3.21, Report No. CERN DD/EE/84-1, 1984, https://inspirehep.net/literature/252007.
- [16] Geant4 Collaboration, Nucl. Instrum. Methods Phys. Res., Sect. A 506, 250 (2003).
- [17] T. Sjostrand, S. Mrenna, and P. Z. Skands, J. High Energy Phys. 05 (2006) 026.
- [18] S. Jadach, B. F. L. Ward, and Z. Was, Comput. Phys. Commun. **130**, 260 (2000).
- [19] S. Jadach, Z. Was, R. Decker, and J. H. Kuhn, Comput. Phys. Commun. 76, 361 (1993).
- [20] M. Gelb et al., Comput. Software Big Sci. 2, 9 (2018).
- [21] T. Kuhr, C. Pulvermacher, M. Ritter *et al.*, Comput. Software Big Sci. 3, 1 (2019).

- [22] T. Kuhr et al. (Belle II Collaboration), Belle II Analysis Software Framework (BASF2), 10.5281/zenodo.5574115 (2021).
- [23] T. Keck, Comput. Software Big Sci. 1, 2 (2017).
- [24] A. Khotanzad and Y. H. Hong, IEEE Trans. Pattern Anal. Mach. Intell. 12, 489 (1990).
- [25] G. C. Fox and S. Wolfram, Phys. Rev. Lett. 41, 1581 (1978).
- [26] G. Punzi, eConf C030908, MODT002 (2003), 10.48550/ arXiv.physics/0308063.
- [27] E. Farhi, Phys. Rev. Lett. 39, 1587 (1977).
- [28] F. Abudinén *et al.* (Belle II Collaboration), Eur. Phys. J. C 82, 283 (2022).
- [29] John E. Angus, SIAM Rev. 36, 652 (1994).
- [30] Kyle S. Cranmer, Comput. Phys. Commun. **136**, 198 (2001).
- [31] H. Albrecht *et al.* (ARGUS Collaboration), Phys. Lett. B **241**, 278 (1990).
- [32] S. Choudhury *et al.* (Belle Collaboration), Phys. Rev. D 107, L031102 (2023).
- [33] For Bayesian upper limits, it is now standard to quote credibility intervals rather than confidence levels, which are appropriate for frequentist analysis [34].
- [34] K. Gray et al., J. Mod. Appl. Stat. Methods 14, 8 (2015).